Journal of Power Sources 195 (2010) 6873–6878

Contents lists available at ScienceDirect

Journal of Power Sources

journal homepage: www.elsevier.com/locate/jpowsour

Porous micro-spherical aggregates of $LiFePO_4$/C nanocomposites: A novel and simple template-free concept and synthesis via sol–gel-spray drying method

Feng Yu[a,b], Jingjie Zhang[a,*], Yanfeng Yang[a], Guangzhi Song[a]

[a] Technical Institute of Physics and Chemistry, Chinese Academy of Sciences, Beijing 100190, China
[b] Graduate University of Chinese Academy of Sciences, Beijing 100049, China

ARTICLE INFO

Article history:
Received 9 October 2009
Received in revised form 21 January 2010
Accepted 21 January 2010
Available online 25 January 2010

Keywords:
Lithium iron phosphate
Cathode material
Porous microsphere
Sol–gel-SD method

ABSTRACT

Porous micro-spherical aggregates of $LiFePO_4$/C nanocomposites were prepared with a process of spray drying at 200 °C and subsequent heat treatment at 700 °C for 12 h by a novel and simple template-free sol–gel-SD method independent of surfactants or templates. The results indicate that the as-obtained $LiFePO_4$ porous microspheres have the mean diameter of 19.8 μm, average pore size of 45 nm, and large specific surface area (20.2 $m^2\,g^{-1}$) with evenly distributed carbon (4.5 wt.%). The particles can be easily brought into contact with electrolyte, facilitating electric and lithium ion diffusion. They present large reversible discharge capacity of 137.5 mAh g^{-1} at the current density of 0.1 C, good rate capacity of 53.8 mAh g^{-1} at 10 C, and excellent capacity retention rate closed to 100% after various current densities in the region of 2.0–4.3 V.

1. Introduction

As a promising cathode material, the polyanionic phosphate compound $LiFePO_4$ has attracted extensive interest among researchers. $LiFePO_4$ with olivine structure possesses excellent structural stability. It exhibits superior performance, including high reversible capacity, acceptable operating voltage, long cycle life, low cost, superior safety and environmental friendliness [1–3]. As has been reported in previous publications [4,5], size reduction in nanocrystalline $LiFePO_4$ leads to a variety of excitation phenomena due to enhanced surface-to-volume ratio and reduced transport length for mobile charges. Nano-sized $LiFePO_4$ particles, synthesized by a number of methods including traditional solid state [6,7], hydrothermal [8,9] and sol–gel methods [10,11], have been found to possess good electrochemical performance. However, nano-sized $LiFePO_4$ particles have the drawback that their high interfacial energy allows them to readily form agglomerations, which seriously impacts their prospect in electrochemical applications. Besides, nano-sized $LiFePO_4$ particles are unfavorable for processing of electrode film on aluminium foil, which needs more agglutinant such as polyvinylidene fluoride (PVDF) than micro-sized $LiFePO_4$ particles [12–14]. Meanwhile, more and more people view and deliberate the risks of nanotechnologies, which may have an impact on human health and the environment [15–19].

We have successfully designed and synthesized porous micro-spherical aggregates of $LiFePO_4$/C nanocomposites by a novel and simple template-free sol–gel-SD method [20]. In the sol–gel-SD method, spray drying technology was employed to deal with gel and to synthesize fine homogeneous and micro-spherical aggregation precursors. It is a promising route that enables quicker evaporation of the gel compared with ordinary evaporation processes and it exhibits superior performance in terms of energy savings, cost effectiveness, continuous preparation, and is environmentally benign [21,22]. At the same time, the relatively low environmental and health risks of porous micro-spherical aggregate of $LiFePO_4$/C nanocomposites make it an increasingly attractive material for nanotechnology applications, which continue to raise greater safety concerns [15,23].

Herein, using the example of $LiFePO_4$/C, we demonstrate the sol–gel-SD route that leads to large (up to 20 μm) primary $LiFePO_4$/C particles, each of which contains organized pores in meso range (45 nm). The as-obtained sample possesses nano-sized, porous and spherical morphology, which allows good electrochemical performance and practical application [20,24]. Compared with other composites formed from nano-sized particles, porous micro-spherical aggregates of $LiFePO_4$/C nanocomposites have the following advantages:

(i) It effectively improves diffusion channels of Li^+ ions by reducing $LiFePO_4$ particle size. In the electrodes consisting of active

* Corresponding author at: Technical Institute of Physics and Chemistry, Chinese Academy of Sciences, Engineering Research Center of Microsphere Materials, PO Box 2711, Beijing 100190, China. Tel.: +86 10 82543691; fax: +86 10 82543691.
E-mail addresses: yufeng05@mail.ipc.ac.cn (F. Yu), jjzhang@mail.ipc.ac.cn (J. Zhang).

0378-7753/$ – see front matter © 2010 Elsevier B.V. All rights reserved.
doi:10.1016/j.jpowsour.2010.01.042

particles, average solid-state diffusion distance (the crucial kinetic parameter) is determined by the average size of the particles [25,26].

(ii) It readily induces the reaction of Fe(III) to Fe(II) by in situ preparation of carbon during heat treatment of appropriate precursor. The carbon can suppress the growth of the $LiFePO_4$ particle during the sintering process, which ameliorates the kinetics of Li^+ intercalation and de-intercalation. Moreover, the diffusion coefficient of electron is greatly improved after incorporating of carbon [10,11,27,28].

(iii) Porous $LiFePO_4$/C particles provide good contact with electrolyte and, in principle, are easier to bind than isolated nano-sized $LiFePO_4$ particles [12,13,24].

(iv) Micro-spherical $LiFePO_4$/C particles are well distributed and do not agglomerate. They have higher safety associated with lower interfacial energy, higher volumetric energy density and better fluidity characteristics. The micro-spherical particles can easily move, closely pack and occupy the available vacancies. In addition, there are no isolated nano-particles which are supposed to present potential health, safety and environmental hazard [25,29,30].

2. Experimental

2.1. Powders preparation

2.1.1. Sol–gel method

Amounts of Li_2CO_3(AR), $Fe(NO_3)_3{\cdot}9H_2O$(AR), H_3PO_4(AR) and tartaric acid were dissolved in distilled water in the stoichiometric ratio—$n_{Li}:n_{Fe}:n_P:n_{acid}$ = 1:1:1:1 to form a homogeneous gel. The gel was burned out at 120 °C for 48 h in an air-limited box furnace, ball-milled for 2 h and then sintered in a tube furnace by using a graphite crucible, heated at 10 °C min^{-1} in flowing argon atmosphere until 700 °C and held for 12 h, then ball-milled for 2 h again to obtain sample LFPa.

2.1.2. Sol–gel-SD method

A homogeneous gel was prepared as in Section 2.1.1, then dispersed in distilled water and made into a suspension without any surfactants or templates. The obtained suspension was spray dried in a spray dryer unit at a rate of 15 mL min^{-1} with inlet and outlet temperatures maintained at 200 °C and 130 °C, respectively. The spray-dried precursor was carbothermally reduced in a tube furnace by using a graphite crucible, heated at 10 °C min^{-1} in a flowing argon atmosphere until 700 °C, then held for 12 h to obtain sample LFPb.

Table 1
Comparison of lattice parameters of the as-obtained samples LFPa and LFPb.

Samples	*a*-Axis (Å)	*b*-Axis (Å)	*c*-Axis (Å)
LFPa	6.0145	10.3431	4.7048
LFPb	6.0320	10.3588	4.7063
Padhi et al. [1]	6.0083	10.3344	4.6931
Barker et al. [31]	5.971	10.288	4.676
JCPDS 40-1499	6.0189	10.3470	4.7039

2.1.3. Sol-SD method

Amounts of Li_2CO_3(AR), $Fe(NO_3)_3{\cdot}9H_2O$(AR), H_3PO_4(AR) and tartaric acid were dissolved in distilled water in the stoichiometric ratio—$n_{Li}:n_{Fe}:n_P:n_{acid}$ = 1:1:1:1 to prepare homogeneous sol, which was spray dried in a spray dryer unit at a rate of 15 mL min^{-1} with inlet and outlet temperatures kept at 200 °C and 130 °C, respectively. Carbothermal reduction of the spray-dried precursor was performed as in Section 2.1.2 to obtain sample LFPc.

2.2. Physical characterization of the synthesized powders

X-ray diffraction (XRD) analysis was carried out on a Rigaku D/max2200PC diffractometer with Cu Kα radiation (λ = 1.5406 Å). The scanning electron microscopy (SEM) images and energy dispersive X-ray (EDX) spectra were obtained using a Hitachi S-4300 microscope and EMAX Horiba, respectively. A Nova 200 Nanolab Dual-beam FIB/SEM instrument was used to obtain inside information of the as-obtained product LFPb. This instrument is a combination of a SEM and a focused ion beam (FIB) with two focused beams in the same location. The FIB instrument is equipped with 30 kV Ga^+ ions with a beam current form 1 pÅ to 20 nÅ. The minimum ion beam spot size is 7 nm at 1 pÅ beam current. A scan-

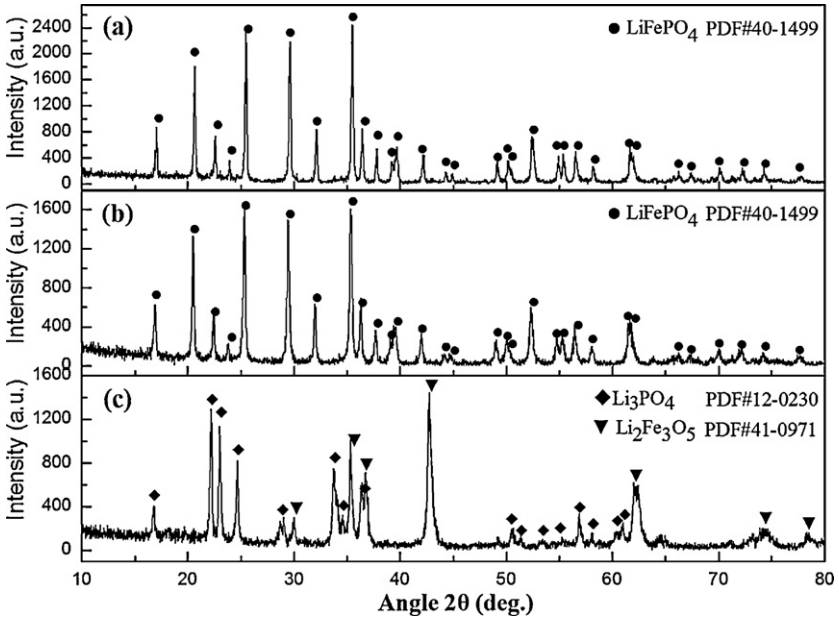

Fig. 1. X-ray diffraction patterns of the as-obtained samples: (a) LFPa, sol–gel method; (b) LFPb, sol–gel-SD method; and (c) LFPc, sol-SD method.

Table 2
Residual carbon content, calculated grain size, specific surface area and coulombic efficiency of the first cycle for the as-obtained samples as a function of the various synthesis methods.

Sample	Synthesis methods	Residual carbon content (wt.%)	Calculated grain size (nm)	Specific surface area ($m^2\ g^{-1}$)	Coulombic efficiency of the first cycle (%)
LFPa	Sol–gel	2.09	48	11.6	91.5
LFPb	Sol–gel-SD	4.48	32	20.2	97.2
LFPc	Sol-SD	0.16	–	–	–

ning probemicroscope in tapping mode was employed to obtain the topographic features. The particle size distribution was measured by a laser diffraction particle size analyzer (Beckman Coulter LS 13 320). The BET specific surface area and pore structure were evaluated by a N_2 adsorption–desorption method using a Quantachrome NOVA 4000 BET apparatus. The elemental analysis of total carbon was performed using a CHNS elemental analyzer Elementar Vario Micro Cube, by which the percentage of the elements in the sorbent can be estimated. The dried and ground sorbent was combusted at 1000 °C. The combustion products (i.e., gases of C) were detected by a thermal conductivity detector for quantitative analysis.

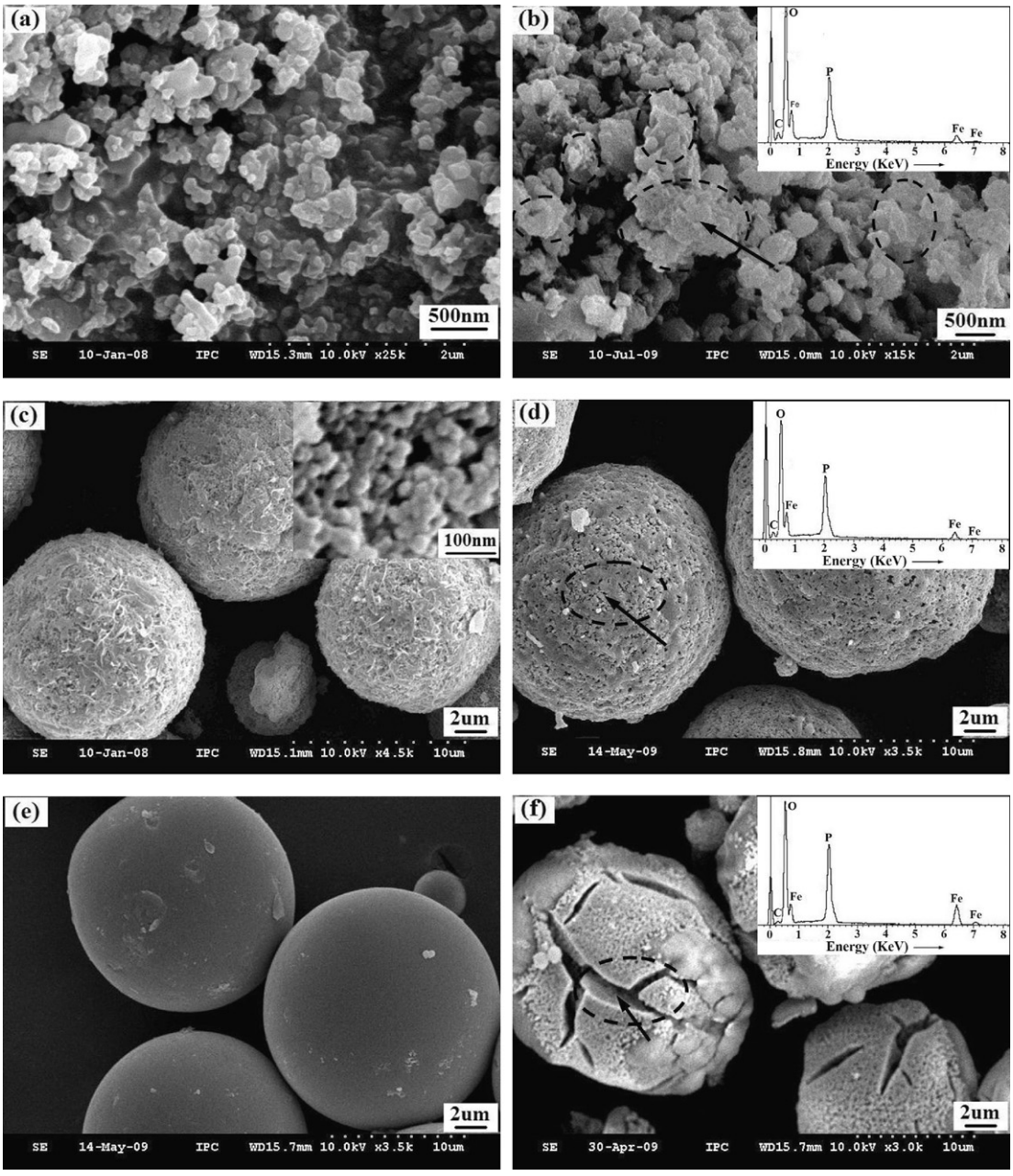

Fig. 2. SEM images of as-obtained precursors and samples using different synthesis method: (a and b) sol–gel method; (c and d) sol–gel-SD method; and (e and f) sol-SD method. Insert in (b), (d) and (f): EDX spectrums of as-obtained samples LFPa, LFPb and LFPc.

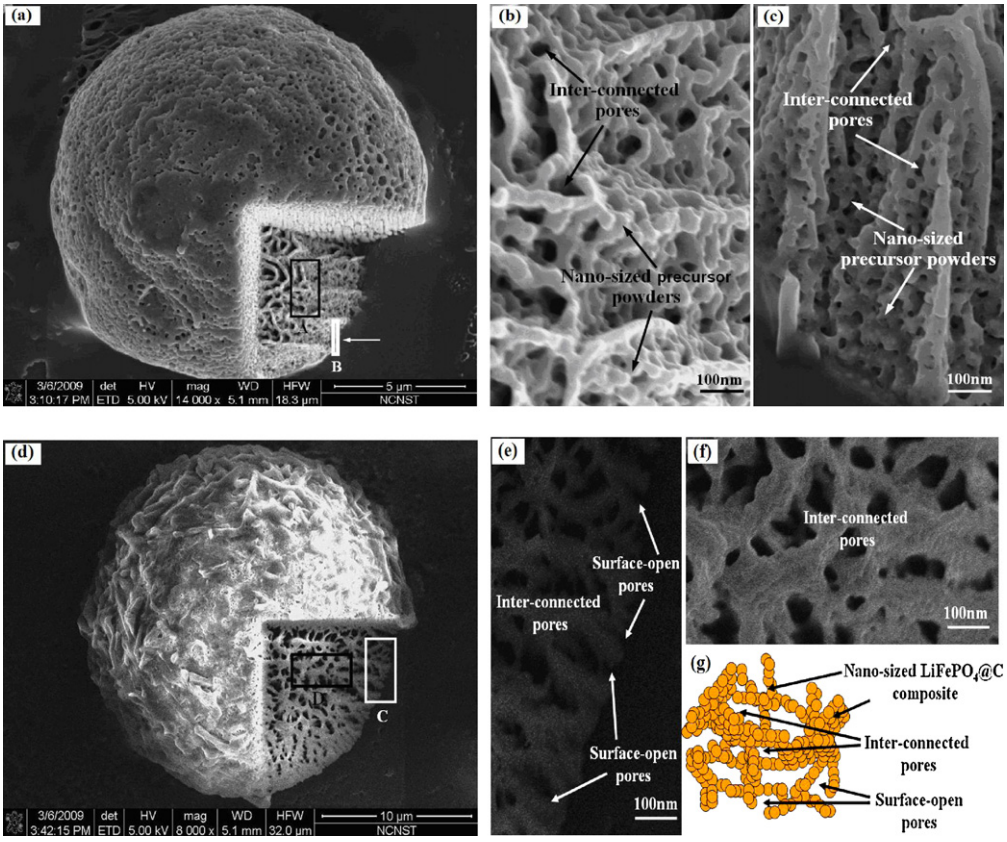

Fig. 3. (a and d) FIB images of the as-obtained precursor and sample LFPb via the sol–gel-SD method. (b) SEM image of area A (indicated by rectangles in panel a). (c) SEM image of area B (indicated by rectangles in panel a). (e) SEM image of area C (indicated by rectangles in panel d). (f) SEM image of area D (indicated by rectangles in panel d). (g) Scheme showing the structure of nano-sized $LiFePO_4$ in a porous micro-spherical aggregate. [20].

2.3. Electrochemical measurement

The electrochemical performance of the as-obtained samples was evaluated using half cell. For fabrication of the working cathodes, the as-obtained samples were mixed with acetylene black (AB) and polyvinylidene fluoride (PVDF) in a weight ratio of 80:15:5 in N-methyl-2 pyrrolidinone (NMP). The obtained slurry was coated onto aluminium foil and dried at 80 °C for 4 h. The dried tape was then punched into round plates with diameter of 10.0 mm and film thickness of 50 μm as the cathode electrodes (5–8 mg loading). The electrodes were dried again at 120 °C for 5 h in a vacuum prior to use. Finally, the prepared cathodes and Celgard2400 separator (diameter of 16.0 mm) were placed into an argon atmosphere filled glove box (H_2O and O_2 < 1 ppm) and assembled into a coin cell (CR2032) with a lithium anode, electrolyte of 1 M $LiPF_6$ in EC-DEC-DMC (1:1:1 vol.%) and the other components of the coin-type cell. The cells were examined with capacity retention studies performed at various rates between 2.0 and 4.3 V. The cells were retained at room temperature for 10 min at 4.3 V in charging.

3. Results and discussion

3.1. Crystalline structure analysis

Fig. 1 compares the X-ray diffraction (XRD) patterns of various as-obtained samples. As seen in Fig. 1a and b, the profiles of the reflection peaks of the as-obtained samples LFPa and LFPb were quite narrow and symmetric. The diffraction lines were all attributed to orthorhombic phase $LiFePO_4$ (JCPDS 40-1499, space group *Pnma*) without any impurity phase. The absolute lattice parameters of the as-obtained samples LFPa and LFPb are listed in Table 1, which are close to the corresponding of JCPDS 40-1499 value and similar to the previous reports [1,31]. No carbon was detected in the XRD pattern, but the result of the energy dispersive X-ray (EDX) analysis confirmed the presence of carbon (see inserts in Fig. 2b and d). It can be easily obtained that the residual carbon content of sample LFPa and sample LFPb is 2.1 wt.% and 4.5 wt.% (Table 2), respectively using an elemental analyzer. It indicates that tartaric acid is decomposed into amorphous carbon during the calcination, and amorphous carbon homogeneously exists in $LiFePO_4$.

Compared with the XRD pattern of the as-obtained sample LFPa, a broadening was seen for the half peak breadth in the XRD

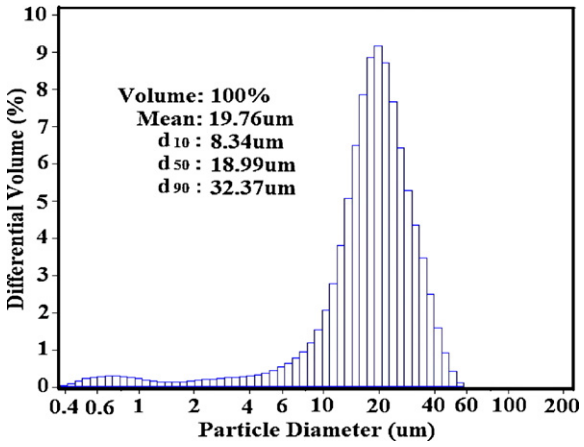

Fig. 4. Particle size distribution of the as-obtained sample LFPb by sol–gel-SD method.

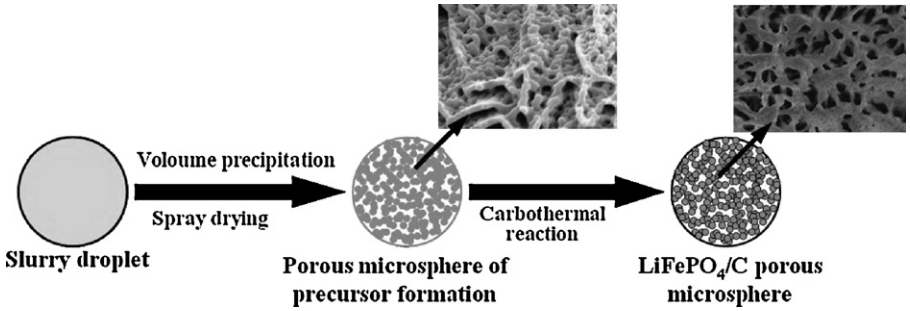

Fig. 5. Description of process from slurry droplet to porous micro-spherical aggregates of $LiFePO_4$/C nanocomposites during spray drying and subsequently carbothermal reaction.

pattern of the as-obtained sample LFPb. Thus, a perfect olivine phase $LiFePO_4$ could be prepared by the sol–gel-SD method, with an estimated crystallite size of the as-obtained sample LFPb of 32 nm (Table 2), which was superior to that of the as-obtained sample LFPa (48 nm, Table 2). The estimated crystallite size was deduced by using the Debye-Scherrer equation and five crystal lattice indexes of (0 1 1), (1 1 1), (1 2 1), (0 3 1) and (1 3 1). However, from the XRD pattern of the as-obtained sample LFPc, prepared by a sol-SD method, the diffraction lines could be attributed to the patterns of Li_3PO_4 (JCPDS 12-0230) and $Li_2Fe_3O_5$ (JCPDS 41-0971), rather than to $LiFePO_4$. A little of residual carbon was confirmed (see insert in Fig. 2f) and its content is only 0.2 wt.% (Table 2).

3.2. Microstructure of the as-obtained samples

Fig. 2 shows the scanning electron microscopy (SEM) images of various precursors and as-obtained samples using various synthesis methods. As seen in Fig. 2a and b, the as-obtained precursor and sample LFPa prepared by the sol–gel method aggregated easily and formed nubbly aggregates even after ball-milling (Fig. 2b, black elliptical area). Irregular aggregates of the as-obtained sample LFPb would seriously hinder its electrochemical performance and practical applications. Fig. 2c is an image of the as-obtained precursor prepared by the sol–gel-SD method without any dispersion treatment, and shows the micro-spherical morphology of the precursor and good uniformity of the morphology. It clearly demonstrates that the micro-spherical aggregates were composed of nano-sized precursor particles. A closer observation of the precursor showed the nano-sized particles building units had a mean diameter of 30 nm (Fig. 2c, insert). After subsequent heat-treating at 700 °C for 12 h, the as-obtained sample LFPb still retains its microspherical morphology with porous structure (Fig. 2d, black elliptical area). The as-obtained precursor prepared by the sol-SD method consisted of well dispersed microspheres with a slippery surface (Fig. 2e), but the as-obtained sample LFPc without $LiFePO_4$ exhibited dissilient micro-spherical morphology (Fig. 2f).

In order to further investigate the morphology and the structural state of the as-obtained sample LFPb and its precursor synthesized by the sol–gel-SD method, a combined system focused ion beam (FIB)/SEM was employed. From the FIB image shown in Fig. 3a, the 3D cross section of the as-obtained precursor microsphere was shown to have a porous structure inside and on the surface. Fig. 3b and c shows obviously inter-connected pores and surface-open pores. This porous micro-spherical aggregation is made of nano-sized precursor particles, which arise from the gel. Even after subsequent heat-treating, the as-obtained sample LFPb remained a porous micro-spherical structure (Fig. 3d), which consisted of $LiFePO_4$/C nanocomposites. As shown in Fig. 3e and f, close observation revealed that inter-connected pores and surface-open pores both consisted of nano-sized $LiFePO_4$/C particles, as shown schematically in Fig. 3g. When filled with electrolyte, these pores highly favor the solid-state diffusion kinetics and are responsible for immediate supply of lithium ions [12,24,32]. The pore diameter (mean 45 nm) and the BET specific surface area (20.2 $m^2\,g^{-1}$, Table 2) measurements were performed with N_2 adsorption–desorption method. The as-obtained sample LFPa synthesized by sol–gel method had smaller surface area (11.6 $m^2\,g^{-1}$, Table 2). The particle size distribution of as-obtained sample LFPb, as shown in Fig. 4, was evaluated by a laser diffraction particle size analyzer. The porous microsphere distribution was essentially a log-normal distribution. The mean size of $LiFePO_4$ porous microspheres was 19.8 μm, which corresponded well with the SEM observation.

To understand the formation mechanism of porous microspherical aggregates of $LiFePO_4$/C nanocomposites, a schematic illustration is proposed in Fig. 5. It mainly consists of two steps. At the first step, an aqueous solution of homogeneous gel was then dissolved in distilled water and formed a suspension liquid. The suspension liquid includes uniformly fine "gel" particulates, which can avoid surface precipitation of droplet during spray drying. When the obtained suspension liquid was spray dried in a spray dryer unit, the volume precipitation carried through in slurry droplet and the uniform nano-sized precursor particles was formed in the slurry droplet [33–35]. At the second step, the carbon from the tartaric acid provided the special environment favorable for the reduction of Fe(III) and the formation of the nanocrystalline composite $LiFePO_4$/C material. Then porous micro-spherical aggregates of $LiFePO_4$/C nanocomposites were formed after heat treating.

3.3. Electrochemical performance

Fig. 6a shows initial charge-discharge profiles of various as-obtained samples at room temperature cycled in the voltage of 2.0–4.3 V at a current rate of 0.1 C. As shown in Fig. 6a, the initial charge-discharge profiles of the as-obtained samples LFPa and LFPb both had a voltage plateau indicative of a typical $LiFePO_4$ [1], while the as-obtained sample LFPc exhibited no voltage plateau. Polarization between the charge and discharge plateaux of as-obtained samples LFPa and LFPb is 84 mV and 57 mV, respectively (insert of Fig. 6a), indicating that the kinetics of the $LiFePO_4$ is indeed improved with more residual carbon coating [32,36]. The initial specific discharge capacities of as-obtained samples LFPa and LFPb are 106.7 mAh g^{-1} and 137.5 mAh g^{-1}, respectively, corresponding to the charge capacities of 116.6 mAh g^{-1} and 141.5 mAh g^{-1}. The calculation shows that the coulombic efficiency during the first cycle of the as-obtained sample LFPa is about 91.5%, which is lower than the value of 97.2% for as-obtained sample LFPb. The as-obtained sample LFPc has no voltage plateau typical $LiFePO_4$ due to the inexistence of $LiFePO_4$.

Cycle stabilities of as-obtained sample LFPb with various discharge current rates are presented in Fig. 6b. The specific discharge capacity decreases with increasing charge/discharge rate and

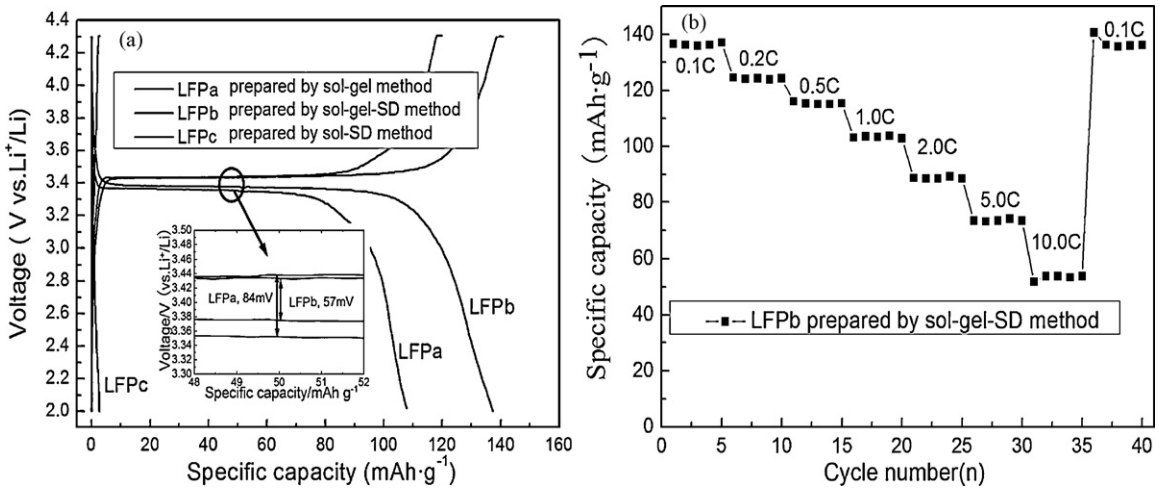

Fig. 6. (a) Initial charge-discharge profiles of various as-obtained samples cycled at a current rate of 0.1 C and (b) the corresponding cyclic stability of the as-obtained product LFPb with various discharge current rates.

reduces to 53.8 mAh g^{-1} at 10 C rate, because lithium diffusion and electronic conduction are limited. When the lower current density was applied, the electrode was able to retrieve its capacity, which confirmed nearly 100% of the starting discharge capability. This retention of sample LFPb on extended cycling shows that it possesses good rate capability and cycle life. It could be attributed to the morphology of porous microsphere and highly uniform distribution of carbon in the $LiFePO_4$ particles.

4. Conclusions

A novel and simple template-free sol–gel-SD method, which is an improved sol–gel method combined with spray drying technology, revealed a way to prepare porous micro-spherical aggregates of $LiFePO_4$/C nanocomposites without employing surfactants or templates. The as-obtained $LiFePO_4$ porous microspheres have average pore size of 45 nm and give large specific surface area (20.2 m^2 g^{-1}) with evenly distributed carbon (4.5 wt.%). It can be easy to bring into contact with electrolyte, facilitate the electric and lithium ion diffusion. They present large reversible discharge capacity of 137.5 mAh g^{-1} at the current density of 0.1 C, good rate capacity of 53.8 mAh g^{-1} at 10 C, and excellent capacity retention rate closed to 100% after various current densities in the region of 2.0–4.3 V. This method provides a simple strategy for quick evaporation of the gel and holds potential for extension to numerous application in porous micro-spherical composites.

Acknowledgements

The authors thank Dr. Kai-Fu Peng (National Center for Nanoscience and Technology, PR China) for his kind help with the FIB/SEM measurements. The authors also thank Dr. Lei Wang (Institute of Mechanics, Chinese Academy of Sciences) for English corrections of this manuscript.

References

[1] A.K. Padhi, K.S. Nanjundaswamy, J.B. Goodenough, J. Electrochem. Soc. 144 (1997) 1188–1194.
[2] M.S. Whittingham, Chem. Rev. 104 (2004) 4271–4302.
[3] D. Jugovic, U. Uskokovic, J. Power Sources 190 (2009) 538–544.
[4] P.G. Bruce, B. Scrosati, J.M. Tarascon, Angew. Chem. Int. Ed. 47 (2008) 2930–2946.
[5] A. Manthiram, A.V. Murugan, A. Sarkar, T. Muraliganth, Energy Environ. Sci. 1 (2008) 621–638.
[6] J.K. Kim, G. Cheruvally, J.W. Choi, J.U. Kim, J.H. Ahn, G.B. Cho, K.W. Kim, H.J. Ahn, J. Power Sources 166 (2007) 211–218.
[7] H.C. Kang, D.K. Jun, B. Jin, E.M. Jin, K.H. Park, H.B. Gu, K.W. Kim, J. Power Sources 179 (2008) 340–346.
[8] H.Y. Yang, X.L. Wu, M.H. Cao, Y.G. Guo, J. Phys. Chem. C 113 (2009) 3345–3351.
[9] E.M. Jin, B. Jin, D.K. Jun, K.H. Park, H.B. Gu, K.W. Kim, J. Power Sources 178 (2008) 801–806.
[10] K.F. Hsu, S.Y. Tsay, B.J. Hwang, J. Mater. Chem. 14 (2004) 2690–2695.
[11] J.K. Kim, J.W. Choi, G.S. Chauhan, J.H. Ahn, G.C. Hwang, J.B. Choi, H.J. Ahn, Electrochim. Acta 53 (2008) 8258–8264.
[12] R. Dominko, M. Bele, M. Gaberscek, M. Remskar, D. Hanzel, J.M. Goupil, S. Pejovnik, J. Jamnik, J. Power Sources 153 (2006) 274–280.
[13] F. Yu, J. Zhang, Y. Yang, G. Song, J. Power Sources 189 (2009) 794–797.
[14] F. Yu, J. Zhang, Y. Yang, G. Song, Chin. J. Inorg. Chem. 25 (2009) 42–46.
[15] R.F. Service, Science 300 (2003) 243.
[16] N. Pidgeon, B.H. Harthorn, K. Bryant, T. Rogers-Hayden, Nat. Nanotechnol. 4 (2008) 95–98.
[17] D.A. Scheufele, E.A. Corley, T.J. Shih, K.E. Dalrymple, S.S. Ho, Nat. Nanotechnol. 4 (2008) 91–94.
[18] Y. Song, X. Li, X. Du, Eur. Respir. J. 34 (2009) 559–567.
[19] A.E. Nel, L. Madler, D. Velegol, T. Xia, E.M.V. Hoek, P. Somasundaran, F. Klaessig, V. Castranova, M. Thompson, Nat. Mater. 8 (2009) 543–557.
[20] F. Yu, J. Zhang, Y. Yang, G. Song, J. Mater. Chem. 19 (2009) 9121–9125.
[21] S.H. Ju, Y.C. Kang, Mater. Chem. Phys. 107 (2008) 328–333.
[22] P. Tewa-Tagne, S. Briancon, H. Fessi, Eur. J. Pharm. Sci. 30 (2007) 124–135.
[23] G. Brumfiel, Nature 424 (2003) 246.
[24] R. Dominko, M. Bele, J.M. Goupil, M. Gaberscek, D. Hanzel, I. Arcon, J. Jamnik, Chem. Mater. 19 (2007) 2960–2969.
[25] M. Gaberscek, R. Dominko, M. Bele, M. Remskar, D. Hanzel, J. Jamnik, Porous, Solid State Ionics 176 (2005) 1801–1805.
[26] P. Balaya, Energy Environ. Sci. 1 (2008) 645–654.
[27] H. Liu, C. Li, H.P. Zhang, L.J. Fu, Y.P. Wu, H.Q. Wu, J. Power Sources 159 (2006) 717–720.
[28] F. Gao, Z. Tang, J. Xue, Electrochim. Acta 53 (2007) 1939–1944.
[29] J. Ying, M. Lei, C. Jiang, C. Wan, X. He, J. Li, L. Wang, J. Ren, J. Power Sources 158 (2006) 543–549.
[30] H.M. Xie, R.S. Wang, J.R. Ying, L.Y. Zhang, A.F. Jalbout, H.Y. Yu, G.L. Yang, X.M. Pan, Z.M. Su, Adv. Mater. 18 (2006) 2609–2613.
[31] J. Barker, M.Y. Saidi, J.L. Swoyer, Electrochem. Solid State Lett. 6 (2003) A53–A55.
[32] Y.S. Hu, Y.G. Guo, R. Dominko, M. Gaberscek, J. Jamnik, J. Maier, Adv. Mater. 19 (2007) 1963–1966.
[33] G.L. Messing, S.C. Zhang, G.V. Jayanthi, J. Am. Ceram. Soc. 76 (1993) 2707–2726.
[34] I. Taniguchi, D. Song, M. Wakihara, J. Power Sources 109 (2002) 333–339.
[35] I. Taniguchi, N. Fukuda, M. Konarova, Powder Technol. 181 (2008) 228–236.
[36] P.P. Prosini, M. Lisi, D. Zane, M. Pasquali, Solid State Ionics 148 (2002) 45–51.